



HOKKAIDO UNIVERSITY

Title	Effects of grain shattering by turbulence on extinction curves in starburst galaxies
Author(s)	Hirashita, Hiroyuki; Nozawa, Takaya; Yan, Huirong et al.
Citation	Monthly Notices of the Royal Astronomical Society, 404(3), 1437-1448 https://doi.org/10.1111/j.1365-2966.2010.16354.x
Issue Date	2010-05
Doc URL	https://hdl.handle.net/2115/44661
Rights	The definitive version is available at www.blackwell-synergy.com
Type	journal article
File Information	2kozasa_MNRAS.pdf



Effects of grain shattering by turbulence on extinction curves in starburst galaxies

Hiroyuki Hirashita,¹★ Takaya Nozawa,² Huirong Yan³ and Takashi Kozasa⁴

¹*Institute of Astronomy and Astrophysics, Academia Sinica, PO Box 23-141, Taipei 10617, Taiwan*

²*Institute for the Physics and Mathematics of the Universe, University of Tokyo, Kashiwa 277-8568, Japan*

³*University of Arizona, LPL, Steward Observatory and Physics Department, 933 N Cherry Avenue, Tucson, AZ 85721, USA*

⁴*Department of Cosmosciences, Graduate School of Science, Hokkaido University, Sapporo 060-0810, Japan*

Accepted 2010 January 13. Received 2010 January 10; in original form 2009 October 11

ABSTRACT

Dust grains can be efficiently accelerated and shattered in a warm ionized medium (WIM) because of the turbulent motion. This effect is enhanced in starburst galaxies, where gas is ionized and turbulence is sustained by massive stars. Moreover, dust production by Type II supernovae (SNe II) can be efficient in starburst galaxies. In this paper, we examine the effect of shattering in a WIM on the dust grains produced by SNe II. We find that, although the grains ejected from SNe II are expected to be biased to large sizes ($a \gtrsim 0.1 \mu\text{m}$, where a is the grain radius), because of the shock destruction in supernova remnants the shattering in a WIM is efficient enough in ~ 5 Myr to produce small grains if the metallicity is nearly solar or more. The production of small grains by shattering steepens the extinction curve. Thus, the steepening of extinction curves by shattering should always be taken into account for systems in which the metallicity is solar and the starburst age is typically greater than 5 Myr. These conditions may be satisfied not only in nearby starburst galaxies but also in high-redshift ($z > 5$) quasars.

Key words: turbulence – supernovae: general – dust, extinction – H II regions – galaxies: evolution – galaxies: starburst.

1 INTRODUCTION

Type II supernovae (SNe II) are considered to be a source of grain production (e.g. Kozasa, Hasegawa & Nomoto 1989; Todini & Ferrara 2001; Nozawa et al. 2003). The significance of SNe II in this respect is enhanced if the cosmic age is young enough (typically at redshift $z > 5$) that low-mass stars, namely asymptotic giant branch (AGB) stars and Type Ia supernovae, cannot contribute significantly to the dust formation (Dwek, Galliano & Jones 2007; but see Valiante et al. 2009), or if the current starburst activity is strong enough. For some nearby blue compact dwarf galaxies (BCDs), the latter condition may be satisfied (Hirashita & Hunt 2004; Takeuchi et al. 2005). Thus, the dust production by SNe II is tested for high- z objects and nearby starburst galaxies.

In galaxies where active star formation (starburst) is occurring, dust grains are produced in and ejected from stars and then processed in the interstellar medium (ISM). In such star-forming galaxies, it is expected that the supernova (SN) rate is enhanced, which leads to an efficient destruction of large grains with $a \gtrsim 0.1 \mu\text{m}$, where a is the grain radius, by SN shocks (e.g. Jones et al. 1994; Jones, Tielens &

Hollenbach 1996). Furthermore, large amounts of ionizing photons are supplied and H II regions develop. Indeed, giant H II regions with sizes of $\gtrsim 100$ pc are found in nearby galaxies (Kennicutt 1984). Such large H II regions are also theoretically expected to occur in a starburst region (Hirashita & Hunt 2004). Moreover, their size is larger than the typical expansion radius of SN shells when the dust condensed in SNe II is finally supplied to the ISM (hereafter N07 Nozawa et al. 2007). Thus, it is reasonable to assume that the dust ejected from SNe II is supplied to the ionized regions in starburst galaxies.

Hirashita & Yan (2009, hereafter HY09) show that shattering occurs efficiently in a warm ionized medium (WIM), where grains are efficiently accelerated by magnetohydrodynamic (MHD) turbulence (Yan & Lazarian 2003; Yan, Lazarian & Draine 2004). The same mechanism is also expected to work in the ionized regions of starburst galaxies. Indeed, turbulence is ubiquitous in the ISM, and the collective effects of OB stellar winds and supernovae (SNe) can play an important role in sustaining turbulence (e.g. Elmegreen & Scalo 2004). Therefore, it is probable that the grains ejected from SNe II into ionized regions are efficiently shattered by turbulence.

Because it has been suggested that large grains with $a \gtrsim 0.1 \mu\text{m}$ are injected into the ISM from SNe II selectively owing to the destruction of small grains in hot plasma caused by the reverse and

★E-mail: hirashita@asiaa.sinica.edu.tw

forward shocks in supernova remnants (SNRs) (N07),¹ shattering in a WIM is important for the production of small grains. If a significant number of small grains are produced, optical–ultraviolet (UV) grain opacity is enhanced, and the slope of the extinction curve becomes steep. In particular, the extinction curves of young starburst galaxies are used to constrain the composition and size distribution of grains formed in SNe II (Maiolino et al. 2004b; Hirashita et al. 2005). Thus, it is important to quantify the effect of grain shattering on the extinction curve.

The production of small grains in starburst environments is also worth investigating in the observational context. The modification of the grain-size distribution should have an impact on dust extinction and emission properties (e.g. Dopita et al. 2005). By studying the spectral energy distributions (SEDs) of the dust and stars of some actively star-forming dwarf galaxies, Galliano et al. (2005) showed that the grain-size distribution is biased to small sizes (\sim a few nanometres). The extinction curves of starburst galaxies in general show a significant reddening in the optical–UV range (Calzetti 2001), indicating that there should be some contribution from small grains. Galliano et al. (2005) also suggest that their results are consistent with the shattering and erosion of ISM grains by SN shocks (Jones et al. 1994, 1996; see also Borkowski & Dwek 1995). Both shock and turbulence are efficient drivers of the relative motion between grains, as the grain acceleration occurs in a way strongly dependent on the grain size (Shull 1977; McKee et al. 1987; Jones et al. 1996; Yan et al. 2004).² At present, however, it is not known which of the two drivers is more important. Thus, in this paper, as a first necessary step to gaining a full understanding of the possible mechanisms of small-grain production, we focus on turbulence as a possible driver of grain shattering.

The paper is organized as follows. We explain the method used in Section 2, and describe some basic results of our calculations in Section 3. We discuss the results and note some observational implications in Section 4. Finally, Section 5 gives the conclusion.

2 METHOD

We consider a young starburst, where dust is predominantly supplied by SNe II. We then calculate the modification of the grain-size distribution by shattering in the WIM. Finally, we examine whether or not the shattering effect is apparent in the extinction curve. In this section, we first explain the initial grain-size distribution in the ejecta from SNe II (Sections 2.1 and 2.2). Next we review the treatment of shattering that was adopted from Jones et al. (1994, 1996) in HY09 (Section 2.3). We use the grain velocities calculated by a MHD turbulence model to obtain the relative grain velocities in shattering (Section 2.4). We also describe the method used to calculate the extinction curve (Section 2.5). Throughout this paper, grains are assumed to be spherical with radius a .

2.1 Initial grain-size distribution

The size distribution of grains ejected from SNe II into the ISM (WIM) is adopted from N07. This size distribution is used as the initial condition for the calculation of shattering in the WIM. N07 have shown that the size distribution of dust formed in the ejecta is

strongly modified by sputtering in ionized gas heated by the reverse and forward shocks. Not only N07 but also Bianchi & Schneider (2007) treat the effect of destruction by shocks in SNe II. N07 consider some aspects that were neglected by Bianchi & Schneider (2007): they solve the motion of dust grains by taking into account the gas drag, and treat the destruction of dust in the radiative phase as well as in the non-radiative phase of SNRs. Thus, we adopt N07’s results for the size distribution of grains ejected from SNe II into the ISM, although the qualitative behaviour of our results are the same even if we adopt the size distribution of Bianchi & Schneider (2007). We also note that both N07 and Bianchi & Schneider (2007) neglect the effects of dust electrical charge and the effects of magnetic fields on grain kinematics. These physical processes, which should be quantified in future work, are discussed further in Section 4.4.

Here we briefly summarize the calculation of N07. N07 started from the grain-size distribution calculated by Nozawa et al. (2003), who treated dust nucleation and growth in SNe II based on the SN model of Umeda & Nomoto (2002). Then, N07 took into account the dust destruction by kinetic and thermal sputtering in hot gas swept up by the reverse and forward shocks after the interaction of the SN ejecta with the ambient ISM. Thus, the grain-size distribution calculated by N07 is regarded as being equal to that injected into the ISM.

N07 treated two extreme cases for the mixing of elements in a SN II: the unmixed case, in which the original onion-like structure of elements is preserved; and the mixed case, in which the elements are uniformly mixed within the helium core. In this paper, we adopt the unmixed case, as the extinction features of carbon and silicon, which are the major grain components in the unmixed case, are consistent with observations (Hirashita et al. 2005; Kawara et al. 2010). Even if the mixed case is adopted, the grain-size distribution is similarly biased to large grain sizes, so that the behaviour of the extinction curve calculated later is expected to be similar.

As a representative progenitor mass, we adopt $20M_{\odot}$, following N07. The grain species formed are C, Si, SiO_2 , Fe, FeS, Al_2O_3 , MgO, MgSiO_3 and Mg_2SiO_4 . According to their calculation, small grains with $a \lesssim 0.02 \mu\text{m}$ are trapped in the shocked region because the deceleration rate of a grain by the gas drag is inversely proportional to its size (e.g. Nozawa, Kozasa & Habe 2006). Thus, these small grains are efficiently destroyed by thermal sputtering if the ambient hydrogen number density, n_{H} , is larger than 0.1 cm^{-3} . Moreover, the destruction efficiency depends sensitively on n_{H} . With n_{H} as large as 10 cm^{-3} , only a few per cent of grains survive, and the grain-size distribution is strongly biased to large ($a \gtrsim 0.1 \mu\text{m}$) radii. It is interesting to note that Slavin, Jones & Tielens (2004) derived similar grain radii for the dynamical decoupling of grains from the interstellar gas, although they include magnetic fields in their calculation (see Section 4.4). The following results on the effects of grain shattering by turbulence in a WIM are not greatly affected by the details in the hydrodynamical treatment of SNe as long as the initial size distribution is biased to large ($a \approx 0.1 \mu\text{m}$) grains.

2.2 Normalization of the grain-size distribution

The total grain mass density integrated for all the size range, ρ_{dust} , is normalized to the gas mass density, $1.4n_{\text{H}}m_{\text{H}}$, to obtain the dust-to-gas ratio, $\mathcal{D} \equiv \rho_{\text{dust}}/(1.4n_{\text{H}}m_{\text{H}})$, where m_{H} is the mass of the hydrogen atom and the factor 1.4 is the correction for species other than hydrogen. Because dust grains are composed of metals, it is useful to label the dust abundance in terms of metallicity. We parametrize the dust abundance by the oxygen abundance, because

¹We call this destruction process ‘destruction in SNRs’.

²Galactic-scale bulk motions such as collective outflow from stellar feedbacks are not efficient at producing the relative motions among grains.

Table 1. Characteristic quantities for SN II dust production for various ambient densities n_{H} .

n_{H} (cm^{-3})	m_{d} (M_{\odot})	\mathcal{D}_0
0.1	0.35	2.2×10^{-3}
1	0.14	8.7×10^{-4}
10	0.033	2.0×10^{-4}

Note. m_{d} is the dust mass ejected per SN II (a progenitor mass of $20M_{\odot}$ is assumed), and \mathcal{D}_0 is the dust-to-gas ratio at the solar metallicity (oxygen abundance) Z_{\odot} .

oxygen is one of the main metals produced by SNe II and oxygen emission lines in the optical are often used to estimate the gas-phase metal abundance. The oxygen mass produced by a SN II of a $20M_{\odot}$ progenitor is $m_{\text{O}} = 1.58 M_{\odot}$ (Umeda & Nomoto 2002). The dust mass after the destruction in SNRs (m_{d}) is listed for each ambient density in Table 1. The solar oxygen abundance is assumed to be $Z_{\odot} = 9.7 \times 10^{-3}$ in mass ratio (Anders & Grevesse 1989). (The oxygen abundance is denoted as Z_{O} and is simply called the metallicity in this paper.) Therefore, in the solar metallicity case, we assume that the dust-to-gas ratio is $\mathcal{D}_0 = Z_{\odot} m_{\text{d}} / m_{\text{O}}$, which is also listed in Table 1. The dust-to-gas ratio is assumed to be proportional to the metallicity: $\mathcal{D} = (Z_{\text{O}} / Z_{\odot}) \mathcal{D}_0$. This is equivalent to the assumption that both dust and oxygen are predominantly supplied from SNe II.

2.3 Shattering

Dust grains are subject to shattering if the relative velocity between grains is larger than 2.7 and 1.2 km s^{-1} for silicate and graphite, respectively (Jones et al. 1996). As shown by Yan et al. (2004), these velocities can be achieved in a magnetized and turbulent ISM. In particular, grains are efficiently accelerated in a WIM, because damping is weak (Yan et al. 2004). The parameters adopted for MHD turbulence and the grain velocities obtained are described in Section 2.4. The time evolution of the grain-size distribution by shattering is calculated by adopting the formulation of Jones et al. (1994, 1996). We briefly review the calculation method. The details are described in HY09.

We solve the shattering equation discretized for the grain size. Although nine grain species are treated here (Section 2.1), the material properties needed for the calculation of shattering are not necessarily available for all species. Thus, we divide the grains into two groups, namely carbonaceous dust and all the other species of dust, and apply the relevant material quantities of graphite and silicate, respectively. In fact, as shown later, the mass and opacity of the latter group are dominated by Si. The validity of this approximation, in which all species other than carbonaceous dust are treated as silicate (called the one-species method), is examined in comparison with another extreme approximation (individual-species method) in Appendix A. Because of the lack of experimental data for Si, we assume that Si (and also the other ‘silicate’ species) can be treated as silicate in shattering because of a similar hardness.³ Because

³Among the materials whose shattering properties are available in table 1 of Jones et al. (1996) (i.e. silicate, SiC, ice, iron and diamond), silicate is expected to have the nearest atomic binding energy to Si. As shown by Serra Díaz-Cano & Jones (2008), who derived the previously unknown shattering properties of hydrogenated amorphous carbon, it is not impossible to estimate relevant quantities, but some guiding quantities from other materials are still necessary even in their method. Thus, here we simply adopt the material quantities of silicate for Si.

the cratering volume in a grain–grain collision is approximately proportional to $1/P_{\text{cr}}$, where P_{cr} is the critical shock pressure for shattering (Jones et al. 1996), the shattering time-scale is roughly proportional to P_{cr} . Thus, if P_{cr} is obtained for appropriate materials (especially Si) in some future experiment, our results can easily be scaled. The material properties of silicate and graphite are taken from Jones et al. (1996) as summarized in HY09.

The number density of grains whose radii are between a and $a + da$ is denoted by $n(a) da$, where the entire range of a is from a_{min} to a_{max} . To ensure the conservation of the total mass of grains, it is convenient to consider the distribution function of grain mass instead of that of grain size. We denote the number density of grains whose masses are between m and $m + dm$ as $\tilde{n}(m) dm$. The two distribution functions are related as $n(a) da = \tilde{n}(m) dm$ and $m = (4\pi/3)a^3 \rho_{\text{gr}}$, where ρ_{gr} is the grain material density (3.3 and 2.2 g cm^{-3} for silicate and graphite, respectively).

For numerical calculation, we consider N discrete bins for the grain radius. The grain radius in the i th ($i = 1, \dots, N$) bin is between $a_{i-1}^{(b)}$ and $a_i^{(b)}$, where $a_i^{(b)} = a_{i-1}^{(b)} \delta$, $a_0^{(b)} = a_{\text{min}}$, and $a_N^{(b)} = a_{\text{max}}$ [i.e. $\log \delta$ specifies the width of a logarithmic bin: $\log \delta = (1/N) \log(a_{\text{max}}/a_{\text{min}})$]. We represent the grain radius and mass in the i th bin as $a_i \equiv (a_{i-1}^{(b)} + a_i^{(b)})/2$ and $m_i \equiv (4\pi/3)a_i^3 \rho_{\text{gr}}$. The boundary of the mass bin is defined as $m_i^{(b)} \equiv (4\pi/3)[a_i^{(b)}]^3 \rho_{\text{gr}}$. Given a_{min} , a_{max} and N , all bins can be set. A grain in the i th bin is called ‘grain i ’. We adopt $a_{\text{min}} = 3 \times 10^{-4} \mu\text{m}$ (3 Å) and $a_{\text{max}} = 3 \mu\text{m}$ to cover the entire grain size range in N07, and $N = 32$. We have confirmed that the results are not altered even if N is doubled.

The mass density of grains contained in the i th bin, $\tilde{\rho}_i$, is defined as

$$\tilde{\rho}_i \equiv m_i \tilde{n}(m_i) \left(m_i^{(b)} - m_{i-1}^{(b)} \right). \quad (1)$$

Note that $\tilde{\rho}_i = \rho_i \delta_i$ in the expression of Jones et al. (1994, 1996). The time evolution of $\tilde{\rho}_i$ by shattering can be written as

$$\left[\frac{d\tilde{\rho}_i}{dt} \right]_{\text{shat}} = -m_i \tilde{\rho}_i \sum_{k=1}^N \alpha_{ki} \tilde{\rho}_k + \sum_{j=1}^N \sum_{k=1}^N \alpha_{kj} \tilde{\rho}_k \tilde{\rho}_j m_{\text{shat}}^{kj}(i), \quad (2)$$

$$\alpha_{ki} = \begin{cases} \frac{\sigma_{ki} v_{ki}}{m_i m_k} & \text{if } v_{ki} > v_{\text{shat}}, \\ 0 & \text{otherwise,} \end{cases} \quad (3)$$

where $m_{\text{shat}}^{kj}(i)$ is the total mass of the shattered fragments of a grain k that enters the i th bin in the collision between grains k and j , σ_{ki} and v_{ki} are, respectively, the grain–grain collision cross-section and the relative collision speed between grains k and i , and v_{shat} is the velocity threshold for shattering to occur. For the cross-section, we apply $\sigma_{ki} = \pi(a_k + a_i)^2$.

The grain velocities given by Yan et al. (2004) are typical velocity dispersions. In order to take into account the directional information, we follow the method in Jones et al. (1994): we divide each time-step into four small steps, and we apply $v_{ik} = v_i + v_k$, $|v_i - v_k|$, v_i and v_k in each small step, where v_i and v_k are the velocities of grains i and k , respectively (see Section 2.4). Note that the mass of the shattered fragment $m_{\text{shat}}^{kj}(i)$ depends on v_{kj} , as described in Jones et al. (1996). Briefly, the total fragment mass is determined by the shocked mass in the collision, and the fragments are distributed with a grain-size distribution $\propto a^{-\alpha_f}$ with $\alpha_f = 3.3$ unless otherwise stated (see HY09 for the size range of the fragments).

For the shattering duration, several mega-years may be appropriate, as this is a typical lifetime of ionizing stars with mass $\gtrsim 20 M_{\odot}$ (lifetime < 10 Myr) (Bressan et al. 1993; Inoue, Hirashita &

Kamaya 2000). HY09 also indicate that the small ($a \lesssim 0.01 \mu\text{m}$) grains depleted by coagulation in dense clouds are recovered if shattering in the WIM lasts for 3–5 Myr, which justifies the necessity of shattering in the WIM for mega-years. We also examine a longer time-scale, 10 Myr, to investigate a starburst environment in which intense star formation occurs continuously. Such a situation may be realized in extragalactic giant ionized regions (Hirashita & Hunt 2004; Hunt & Hirashita 2009). In summary, we examine $t = 3, 5$ and 10 Myr, where t is the elapsed time of shattering.

2.4 Grain velocity

The grain velocity as a function of grain radius a in the presence of interstellar MHD turbulence is calculated using the method described in Yan et al. (2004). They considered the grain acceleration by hydrodrag and gyroresonance and calculated the grain velocities achieved in various phases of the ISM. Among the ISM phases, we focus on the WIM to investigate the possibility of efficient shattering in actively star-forming environments.

We adopt three cases for the hydrogen number density of the WIM ($n_{\text{H}} = 0.1, 1$ and 10 cm^{-3}), as N07 applied these densities for the ambient medium. For the WIM, a density of $n_{\text{H}} \sim 0.1\text{--}1 \text{ cm}^{-3}$ is usually considered (McKee & Ostriker 1977), but we also examine a density as high as $n_{\text{H}} \sim 10 \text{ cm}^{-3}$ for young H II regions around massive stars, as observed in starburst environments (Hunt & Hirashita 2009). Embedded starburst regions may also have such dense ionized regions. We adopt a gas temperature $T = 8000 \text{ K}$, an electron number density $n_e = n_{\text{H}}$, an Alfvén speed $V_A = 20 \text{ km s}^{-1}$ and an injection scale of the turbulence $L = 100 \text{ pc}$, following Yan et al. (2004). The effect of the injection scale is minor compared with that of the sound and Alfvén velocities. Because both the sound speed and the Alfvén speed are fixed, the plasma β is constant in all cases. The grain charge is assumed to be the same as that in Yan et al. (2004), who calculated it by assuming a typical Galactic condition. Because we expect a higher value for the interstellar radiation field and a higher electron density for starburst environments, the absolute values for the grain charge can be larger than those assumed here. For grains with $a \gtrsim 0.1 \mu\text{m}$, where most of the grain mass is contained in our cases, the grain velocity is governed by the gyroresonance. The acceleration rate of gyroresonance increases with the grain charge, but the acceleration duration, the

gaseous drag time, decreases with the grain charge (Yan & Lazarian 2003). As a result, the acceleration efficiency of gyroresonance is insensitive to the grain charge.

In Fig. 1, we show the grain velocities. In general, larger grains tend to acquire larger velocities because they are coupled with larger-scale motions. For small grains, the motion is governed by the gaseous drag, which has a linear dependence on the grain charge (Yan et al. 2004). This is the reason for the complex (non-monotonic) behaviour of the grain velocity as a function of a for small grains ($< 0.1 \mu\text{m}$). We also observe that the grain velocity is not very sensitive to n_{H} for large ($a \gtrsim 0.1 \mu\text{m}$) grains, whose shattering is important in this paper.

2.5 Extinction curves

Extinction curves have been an effective tool with which to examine dust properties (e.g. Mathis 1990). For the calculation of extinction curves, we adopt the same optical constants as in Hirashita et al. (2008) for the grain species formed in SNe II (C, Si, SiO_2 , Fe, FeS, Al_2O_3 , MgO, MgSiO_3 and Mg_2SiO_4). The grain properties of individual species and the references for the optical constants are listed in table 1 of Hirashita et al. (2008). Using these optical constants, we calculate the absorption and scattering cross-sections of homogeneous spherical grains with various sizes based on the Mie theory (Bohren & Huffman 1983). Then, the grain extinction coefficient as a function of wavelength is obtained by weighting the cross-sections with the grain-size distribution. The total extinction as a function of wavelength λ , denoted as A_λ , is calculated by summing the contributions from all species.

As stated in Section 2.3, we divide the grain species into two groups in the calculation of shattering: carbonaceous dust and silicate, which in fact contains all species other than carbonaceous dust. In the calculation of the extinction curves, the size distribution of the silicate species is redistributed to each component (Si, SiO_2 , Fe, FeS, Al_2O_3 , MgO, MgSiO_3 and Mg_2SiO_4) in proportion to the grain volume (i.e. the total mass of each component divided by its material density) with a fixed shape of the grain-size distribution. In fact, Si is dominant in the extinction curve, so the uncertainty resulting from the above rough treatment does not affect our conclusion (Appendix A).

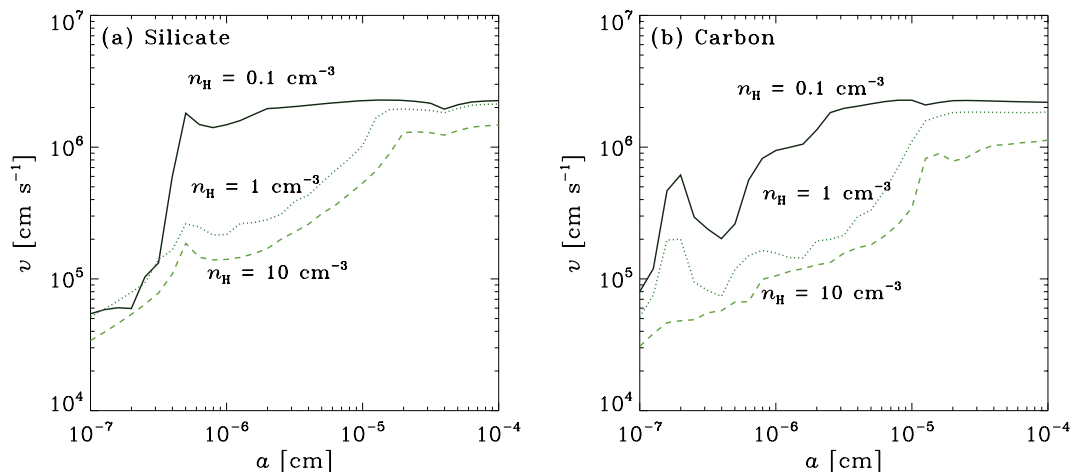


Figure 1. Grain velocities v calculated from the turbulence model as a function of grain radius a . Two grain species, (a) silicate and (b) carbonaceous dust, are shown. The solid, dotted and dashed lines indicate the velocities with hydrogen number densities of $n_{\text{H}} = 0.1, 1$ and 10 cm^{-3} , respectively.

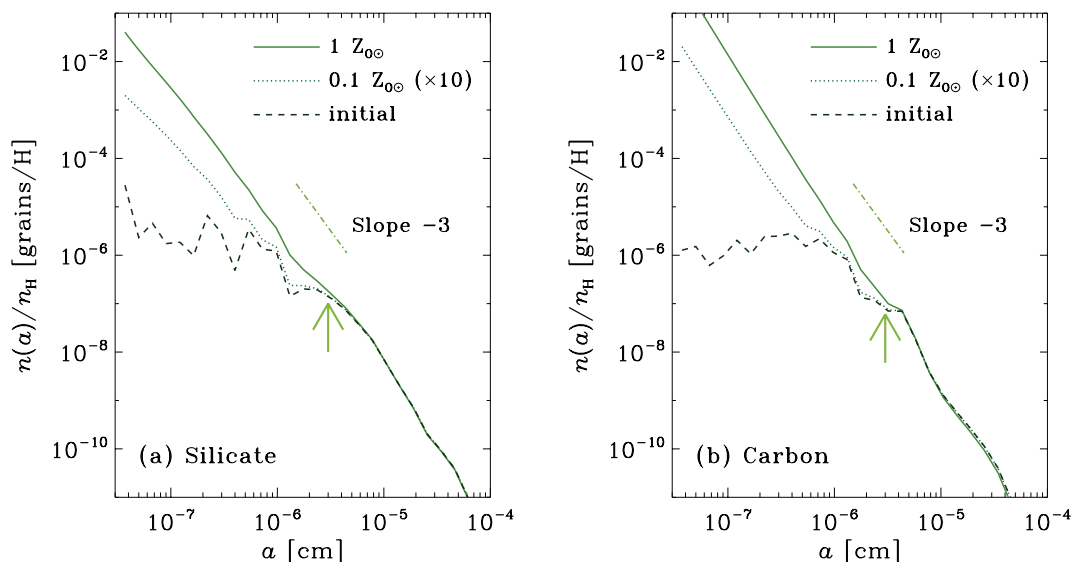


Figure 2. Grain-size distributions per hydrogen atom. The solid and dotted lines show the results at $t = 5$ Myr for metallicities of $1Z_{\odot}$ and $0.1Z_{\odot}$, respectively. The hydrogen number density n_{H} is assumed to be 0.1 cm^{-3} . The dashed line presents the initial grain-size distribution before shattering. Two grain species, (a) silicate and (b) carbonaceous dust, are shown. The case with $0.1Z_{\odot}$ is multiplied by 10 for display purposes to offset the 10-times smaller dust abundance. The arrow at $a = 0.03 \mu\text{m}$ is a rough representative size of the grains contributing to the steepening of the UV extinction curve.

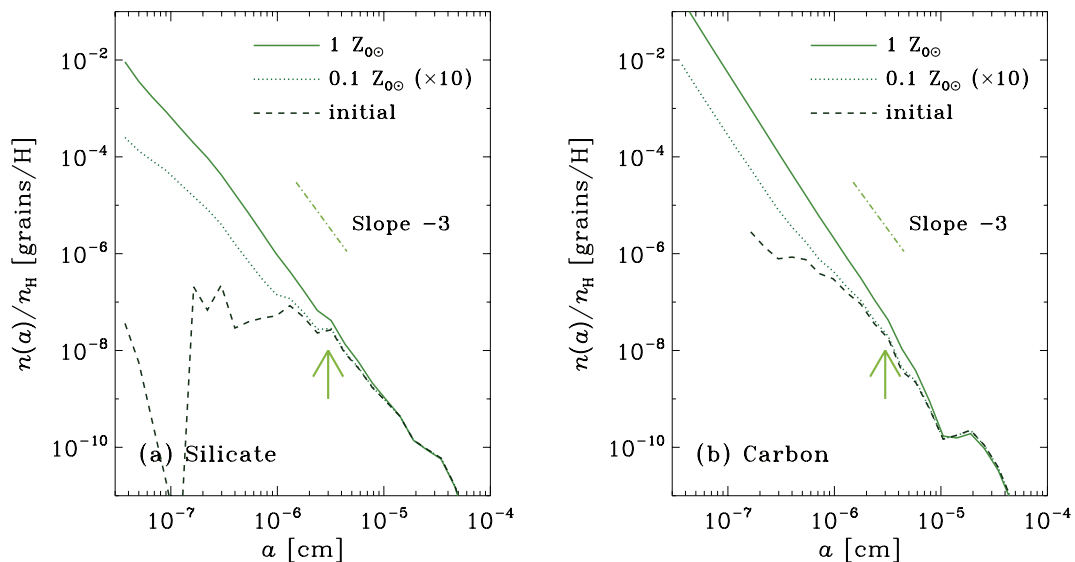


Figure 3. As Fig. 2, but for $n_{\text{H}} = 1 \text{ cm}^{-3}$.

3 RESULTS

3.1 Grain-size distribution after shattering

The grain-size distributions after shattering are shown in Figs 2–4 for $n_{\text{H}} = 0.1, 1$ and 10 cm^{-3} , respectively. The grain-size distribution is shown by $n(a)/n_{\text{H}}$. We adopt $t = 5$ Myr as a typical time-scale on which the WIM is sustained by the radiation from massive stars (Section 2.3). Two cases for the metallicity, $Z_{\odot} = 0.1$ and $1 Z_{\odot}$, are examined.

We observe that shattering affects the grain-size distribution for all densities. In particular, the abundance of small grains with $a \lesssim 0.1 \mu\text{m}$ significantly increases after the shattering of a small portion

of larger grains. If the metallicity is $1Z_{\odot}$, a continuous power-law-like size distribution is realized for $a \lesssim 0.1 \mu\text{m}$. Although the dust abundance is lower for higher n_{H} (Table 1), because of more efficient shock destruction in the SN remnant before the ejection to the ISM (N07), the grain–grain collision rate is enhanced in environments with higher n_{H} .

The increase of grains with $a \lesssim 0.1 \mu\text{m}$ could have a strong effect on the UV and optical extinction curves. This point is quantitatively addressed in Section 3.2. Large grains with $a > 0.1 \mu\text{m}$ are marginally affected by shattering; that is, the shattering of a small fraction of large grains can produce a large number of small grains. In the case of HY09, on the other hand, grains with $a > 0.1 \mu\text{m}$ are more shattered because abundant small grains in the MRN (Mathis,

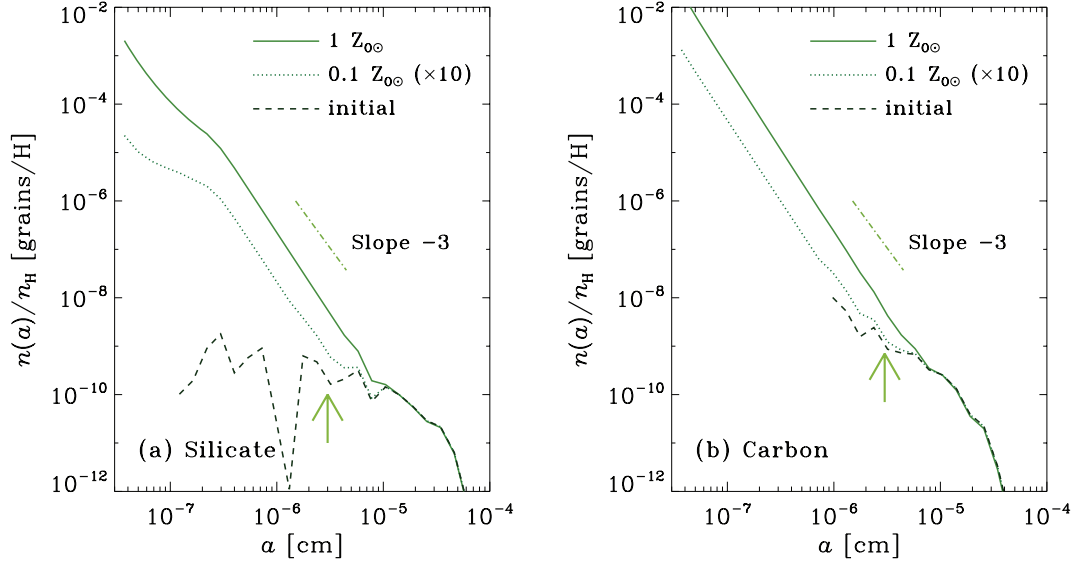


Figure 4. As Fig. 2, but for $n_{\text{H}} = 10 \text{ cm}^{-3}$.

Rumpl & Nordsieck 1977) grain-size distribution, which they assumed as the initial condition, enhance the grain–grain collision rate.

3.2 Extinction curves

The extinction curve of grains ejected from SNe II tends to be flat because small grains are efficiently destroyed in SNRs before they

can escape into the ISM (Hirashita et al. 2008). Here we investigate whether or not the increase of small grains by shattering effectively steepens the extinction curves.

In Fig. 5, we show the time variation of extinction curves for $n_{\text{H}} = 0.1, 1$ and 10 cm^{-3} with $Z_{\text{O}} = 1 Z_{\odot}$. We normalize the extinction to A_{V} (i.e. at $\lambda = 0.55 \mu\text{m}$). As stated by Hirashita et al. (2008), the initial extinction curve is steeper for lower n_{H} ,

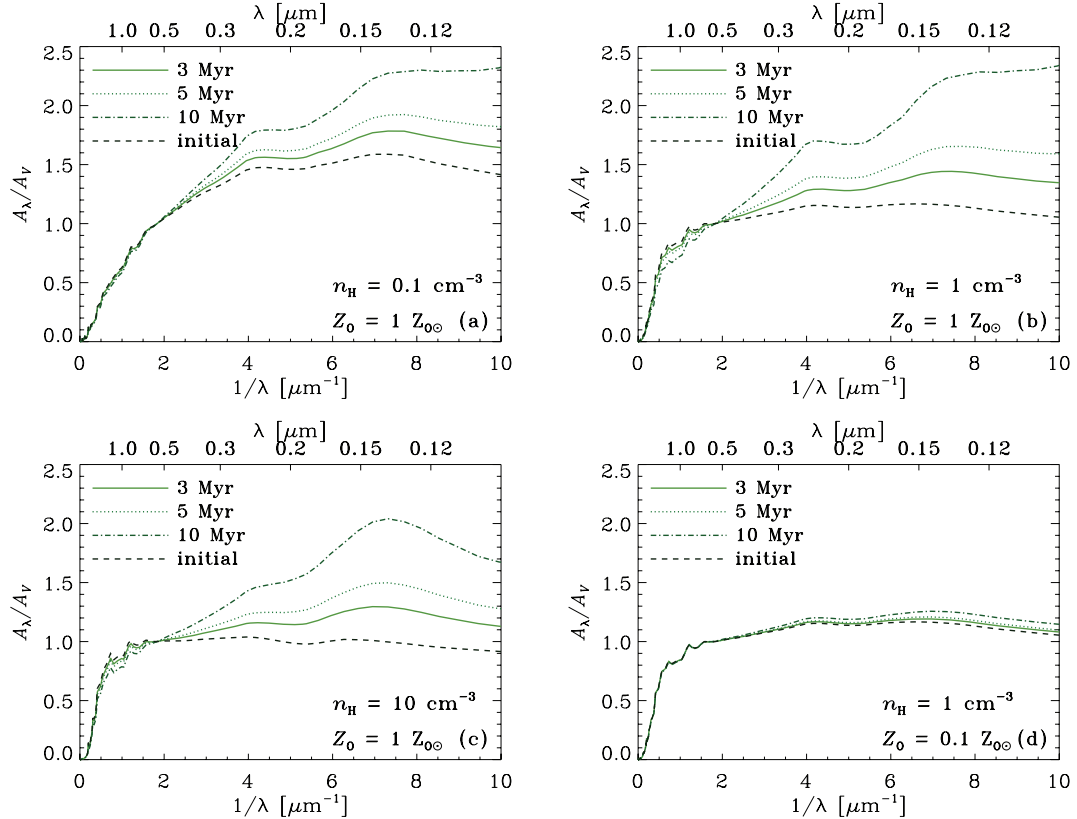


Figure 5. Extinction curves normalized to the V-band extinction. The solid, dotted and dot–dashed lines indicate the results at $t = 3, 5$ and 10 Myr , respectively. Panels (a), (b) and (c) present the results for $n_{\text{H}} = 0.1, 1$ and 10 cm^{-3} , respectively, with $Z_{\text{O}} = 1 Z_{\odot}$. Panel (d) shows the result for $n_{\text{H}} = 1 \text{ cm}^{-3}$ with $Z_{\text{O}} = 0.1 Z_{\odot}$.

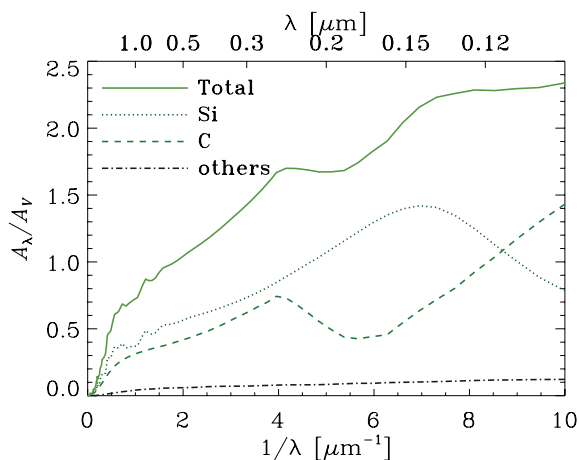


Figure 6. Contributions from Si, C and the other grain species (dotted, dashed, and dot-dashed lines, respectively) for the case of Fig. 5(b) ($n_{\text{H}} = 1 \text{ cm}^{-3}$ and $Z_{\text{O}} = 1 Z_{\odot}$) at $t = 10 \text{ Myr}$. The solid line shows the total extinction.

as more small grains survive after the shock destruction in SNRs. We also observe that the extinction curve becomes steeper as the grains are shattered for a longer time because of the production of small grains. Indeed, at $t = 5 \text{ Myr}$, A_{λ}/A_V at $\lambda \sim 0.2 \mu\text{m}$ increases by more than 20 per cent for $n_{\text{H}} = 1 \text{ cm}^{-3}$. The variation of the slope by shattering is more pronounced for larger n_{H} , as the original extinction curve is flatter.

The extinction curves are dominated by Si and C, which survive after the shock destruction in SNRs because of their relatively large sizes (N07). Therefore, the steepening of the extinction curve results mainly from the production of small Si and C grains by shattering. The contributions from Si, C and the other species are shown in Fig. 6. The ‘bump’ features at $1/\lambda \sim 4$ and $7 \mu\text{m}^{-1}$ originate from the absorption by C and Si, respectively. Such features tend to be prominent for smaller grains, because as grains become larger the extinction cross-sections are determined more by the geometrical ones, not by the grain properties (Bohren & Huffman 1983). Thus, not only the steep slope but also various features in the extinction curve become apparent as grains are subject to shattering.

We also examine the dependence on the dust abundance (metallicity). In Fig. 5(d), we show the evolution of the extinction curve for $Z_{\text{O}} = 0.1 Z_{\odot}$. The effect of shattering is significantly reduced compared with the case of solar metallicity. If the grain velocity as a function of grain size is fixed, a constant $Z_{\text{O}}t$ gives the same result. Thus, if Z_{O} is 10 times lower, a time 10 times longer is required for the same shattering effect to appear. The scaling with $Z_{\text{O}}t$ is useful if one would like to know the results for other time-scales and/or metallicities.

4 DISCUSSION

4.1 Steepening of the UV extinction curve

In the above section, we showed that the abundance of small ($a < 0.1 \mu\text{m}$) grains increases through the shattering of large ($a \gtrsim 0.1 \mu\text{m}$) grains. Consequently, the slope of the UV extinction curve becomes steep after shattering. Here, we discuss this phenomenon in terms of the grain-size distribution.

The contribution from grains in a logarithmic size range $[\ln a, \ln a + d \ln a]$ to the extinction can be written as

$d\kappa_{\text{ext}} \equiv \pi a^2 Q_{\lambda}(a) n(a) a d \ln a$, where $Q_{\lambda}(a)$ is the extinction cross-section normalized to the geometrical cross-section (πa^2). If the size distribution is approximated by a power law ($n \propto a^{-p}$) over a certain size range, $d\kappa_{\text{ext}}/d \ln a \propto a^{3-p} Q_{\lambda}(a)$. Because $Q_{\lambda}(a) \sim 1$ for $2\pi a \gtrsim \lambda$ and $Q_{\lambda}(a) \propto a$ for $2\pi a \ll \lambda$ (e.g. Bohren & Huffman 1983), we obtain $d\kappa_{\text{ext}}/d \ln a \propto a^{3-p}$ for $2\pi a \gtrsim \lambda$ and $d\kappa_{\text{ext}}/d \ln a \propto a^{4-p}$ for $2\pi a \ll \lambda$. Thus, if $p < 3$, the largest grains make the largest contribution to the extinction. In order for small grains to make a significant contribution to the extinction, $p \geq 3$ should be satisfied. If $3 < p < 4$, the largest contribution to the extinction comes from the grains with $2\pi a \sim \lambda$. In other words, the UV ($\lambda \sim 0.2 \mu\text{m}$) extinction curve is steepened significantly if grains with $a \sim 0.03 \mu\text{m}$ are produced and $p \gtrsim 3$ is satisfied around this grain size.

From Figs 2–4, we observe that a large number of grains with $a \sim 0.03 \mu\text{m}$ are produced, and the slope around this grain radius is $p \gtrsim 3$ for the solar metallicity cases. Indeed, the UV slope of the extinction curve is steepened for the solar metallicity cases, as shown in Fig. 5.

In this paper, the shattered fragments are distributed with a size distribution with exponent $\alpha_f = 3.3$ (Section 2.3). Jones et al. (1996), from a discussion on the cratering flow, argue that a value of α_f slightly larger than 3 is robust. Even if $\alpha_f = 2.5$ is assumed as an extreme case, the difference in the extinction curve is less than 10 per cent at $\lambda = 0.1 \mu\text{m}$ and smaller at longer wavelengths (see Appendix B for details).

4.2 Grain properties in starburst environments

From the results above, the presence of small grains in starburst environments is generally predicted, although SNe II tend to eject large grains because of the shock destruction in SNRs. For example, BCDs (or H II galaxies) in the nearby Universe host large ionized regions, and the age of the current star-formation episode is a few Myr to 20 Myr (e.g. Hirashita & Hunt 2004; Takeuchi et al. 2005). These ages are just in the range where shattering could modify the grain-size distribution and extinction curve, although we should take into account the low metallicity in BCDs. Some BCDs show an excess of near-infrared emission (e.g. Hunt, Vanzi & Thuan 2001), which can be attributed to the emission from transiently heated very small grains (Aannestad & Kenyon 1979; Sellgren 1984; Draine & Anderson 1985). Galliano et al. (2005) carried out a comprehensive analysis of the SEDs of dust and stars in some dwarf galaxies (dwarf irregular galaxies and BCDs), and showed that the grain size is biased to small grains with radii of a few nanometres. Because their sample galaxies have metallicities larger than $1/10 Z_{\odot}$, shattering in the WIM can work as a production source of nanometre-sized grains on time-scales of a few mega-years, and thus can be considered as an origin of small grains in these galaxies.

It is natural to expect that a similar condition (i.e. turbulence in a WIM sustained for more than a few mega-years) is generally realized in starburst galaxies. Although it is hard to compare the extinction curve with the observed wavelength dependence of the dust attenuation because of the effects of radiative transfer (Calzetti 2001; Inoue 2005), shattering may be crucial to reproducing the reddening observed in starburst galaxies. Therefore, shattering should be considered as a source of small grains, which contribute to the reddening. Alternatively, dust produced by AGB stars in the underlying old population (older than several $\times 10^8 \text{ yr}$; Valiante et al. 2009) could contribute to the steepening if they produce small grains; however, there are some observational indications that dust

grains produced in AGB stars are large ($a \sim 0.1 \mu\text{m}$) (Groenewegen 1997; Gauger et al. 1999).

Efficient shattering also occurs in the ISM by means of the passage of SN shocks. Jones et al. (1996) show that a large fraction of large grains with $a > 0.1 \mu\text{m}$ is redistributed into smaller grains by a single passage of a shock with a velocity of $\sim 100 \text{ km s}^{-1}$. In their calculation, large grains take a longer time before they are dynamically coupled with gas and are subject to more collisions with dust. Jones et al. (1996) consider the MRN distribution as the initial grain-size distribution, which enhances the shattering efficiency compared with our case, because of the enhanced collision with the abundant small grains. Below, we estimate the time-scale on which shattering in SN shocks destroys large grains based on Jones et al. (1996), although the time-scale obtained might be an underestimate for the grains produced by SNe II, because of the enhanced collision rate in the MRN distribution.

The time-scale on which shattering in SN shocks effectively destroys large grains can be estimated in a way similar to in McKee (1989). A single SN can sweep $M_{\text{sw}} \sim 10^4 M_{\odot}$ of gas (i.e. $M_{\text{sw}} v_s^2/2 \sim E_{\text{SN}}$, with shock velocity $v_s \sim 100 \text{ km s}^{-1}$ and the energy given to the gas by a SN equal to $E_{\text{SN}} \sim 10^{51} \text{ erg}$). Then, the gas mass swept by SN shocks with $v_s \gtrsim 100 \text{ km s}^{-1}$ per unit time can be estimated as $M_{\text{sw}} \gamma$, where γ is the SN rate. Thus, the time-scale on which the entire gas mass M_g is affected by shattering by SN shocks is estimated as $\tau_{\text{sw}} \sim M_g/(M_{\text{sw}} \gamma)$. Because $\gamma/\psi \sim 10^{-2} M_{\odot}^{-1}$ for a Salpeter initial mass function (Salpeter 1955) (ψ is the star-formation rate), the above time-scale is estimated as $\tau_{\text{sw}} \sim 10^{-2} M_g/\psi$. This estimate indicates that the shattering time-scale by SN shocks is about 0.01 times the gas consumption time-scale by star formation. In starburst environments, $M_g/\psi \sim 10^8\text{--}10^9 \text{ yr}$ may be reasonable (Young et al. 1986), and shattering in SN shocks occurs in 1–10 Myr, which is comparable to the time-scale investigated in this paper. Therefore, both shattering in turbulence and that in SN shocks can affect the grain-size distribution. A detailed calculation of shattering in SN shocks of grains produced by SNe II is required before we judge which of these two shattering mechanisms is dominant.

It might also be useful to discuss our results in terms of the extinction curves of the Large and Small Magellanic Clouds (LMC and SMC), both of which have developed H II regions such as 30 Doradus. Indeed, Bernard et al. (2008) indicate that the 70- μm excess around 30 Doradus can be explained by an enhancement of the abundance of very small grains, possibly by the destruction of large grains. Bot et al. (2004) find this excess in the SMC. Paradis et al. (2009) show that the very small grain abundance is substantially enhanced around 30 Doradus using an SED model of dust emission. However, the extinction curves in these galaxies are much steeper than our results ($A_{\lambda}/A_V \simeq 2.9$ and 3.2 at $\lambda \simeq 0.2 \mu\text{m}$ for the LMC and the SMC, respectively; Pei 1992). Because these galaxies have less intense star formation than BCDs, non-starbursting components are likely to contribute significantly to the extinction curve. The steep extinction curves of the LMC and the SMC indicate that we should consider not only the dust production/shattering in star-forming regions but also various other mechanisms that act as efficient production sources of small grains. For example, shattering in a warm *neutral* medium works on a time-scale of 100 Myr (HY09). ISM phase exchange, which occurs on a time-scale of 50–100 Myr, also affects the evolution of the grain-size distribution (O’Donnell & Mathis 1997). Such longer-time-scale mechanisms could also have affected the extinction curves (grain-size distributions) of those galaxies. The current paper, which focuses on a

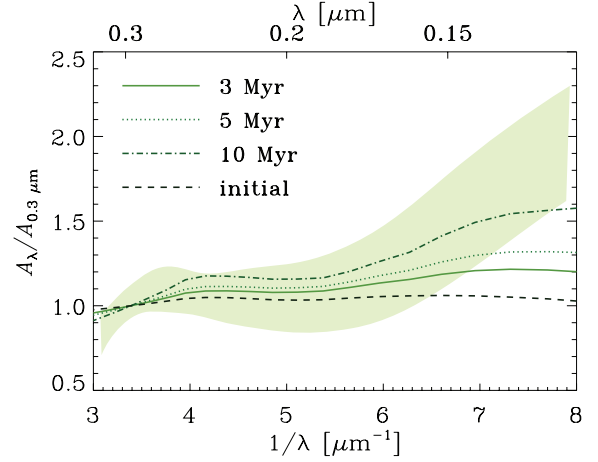


Figure 7. The extinction curves in Fig. 5(b) plotted only in the UV range ($Z_{\odot} = 1 Z_{\odot}$ and $n_{\text{H}} = 1 \text{ cm}^{-3}$). The shaded area shows the observed extinction curve for SDSS J1048+4637 ($z = 6.2$) by Maiolino et al. (2004b), including the uncertainty.

short-time-scale ($< 10 \text{ Myr}$) grain processing, is a starting point for the inclusion of other physical processes in future work.

4.3 Comparison with high- z data

At $z > 5$, it is usually assumed that the main production source of dust is SNe II, whose progenitors have short lifetimes, as the cosmic age is too young for low-mass stars to evolve (but see Valiante et al. 2009). Thus, the extinction curves at such high z are often used to test the theory of dust production in SNe II (Maiolino et al. 2004b; Hirashita et al. 2005). As a representative case of observed high- z extinction curve, we discuss the rest-frame UV extinction curve of SDSS J1048+4637 ($z = 6.2$) obtained by Maiolino et al. (2004b).

In Fig. 7, we show the UV part of the extinction curves calculated with our models in comparison with the observed UV extinction curve of SDSS J1048+4637. The extinction curves are normalized to the value at $\lambda = 0.3 \mu\text{m}$. We show the result for $n_{\text{H}} = 1 \text{ cm}^{-3}$, but the following discussions hold qualitatively also for other densities. As discussed in Hirashita et al. (2008), the initial extinction curve before shattering is too flat to explain the UV rise in the observed extinction curve because small grains are selectively destroyed in SNRs. However, after shattering, the extinction curve approaches the observed curve because of the production of small grains. After 10 Myr of shattering, the observed extinction curve is reproduced. Not only the slope but also the bump feature at $1/\lambda \sim 4 \mu\text{m}^{-1}$, which becomes prominent after shattering (Section 3.2), may account for the behaviour of the observed extinction curve around $1/\lambda \sim 3.5\text{--}4 \mu\text{m}^{-1}$.

In summary, if the metallicity is nearly solar and the age of the current episode of starburst is greater than 5 Myr, we should take the effect of shattering in turbulence into account when comparing the observed extinction curve with the theoretical one, even at $z > 5$. Because quasars tend to be found in evolved stellar systems whose metallicity could be nearly solar (or more than solar; Juaerz et al. 2009), the UV rise of the extinction curve may be caused by the production of small grains by shattering. The dependence of the extinction curve on age and metallicity may also be responsible for the variation of the UV slope of the quasar spectra in the sample of Maiolino et al. (2004a).

4.4 Remarks on grain physics

Before concluding this paper, we mention some physical processes to be considered in the future. In the calculation of the shock destruction of grains in SNRs by N07, the effects of grain electrical charge and the effects of magnetic fields are ignored. As shown in Jones et al. (1994, 1996) and more recently by Guillet, Pineau Des Forêts & Jones (2007) and Guillet, Jones & Pineau Des Forêts (2009), the dynamics of charged grains is critically modified by magnetic fields. The gyration around the magnetic fields tends to strengthen the coupling between gas and dust, and this effect could suppress the ejection of large grains into the ISM. Thus, not only small grains but also large grains with $a \gtrsim 0.1 \mu\text{m}$ could be subject to significant processing in the shock. Slavin et al. (2004) show that the presence of magnetic fields in shocks produces complexity in the kinematics of large ($\gtrsim 0.1 \mu\text{m}$) grains. Thus, it may be important to trace the grain trajectory around the reverse and forward shocks. The quantification of all these effects of magnetic fields is left for future work.

The importance of shattering by turbulence for small-grain production in starburst galaxies should, however, still be considered even if we take into account the effect of the magnetic field in the future, because it is still true that the shock destruction in SNRs suppresses the injection of small grains into the ISM. It should also be kept in mind that at the smallest size ranges (a few Å), the treatment of grains as a bulk solid may not be a good approximation. Because such tiny grains do not affect the UV–optical extinction curve, as discussed in Section 4.1, the results on the extinction curves are not affected. Mid-infrared spectra of dust emission are more suitable for constraining the abundance of such small grains (e.g. Mathis 1990).

5 CONCLUSION

We have theoretically investigated the effect of shattering in a turbulent WIM on the grain-size distribution using the framework for shattering developed by Jones et al. (1994, 1996) and the calculation of interstellar MHD turbulence obtained by Yan et al. (2004). We have focused on systems in which dust is predominantly produced by SNe II. Although SNe II tend to eject large ($a \gtrsim 0.1 \mu\text{m}$) grains because of the shock destruction in SNRs (N07), shattering in the WIM supplies small grains on a time-scale of several mega-years in the solar-metallicity (i.e. Galactic dust-to-gas ratio) case. Consequently, the extinction curve is steepened and the features such as the carbon bump around $1/\lambda \sim 4 \mu\text{m}^{-1}$ and the Si bump around $1/\lambda \sim 7 \mu\text{m}^{-1}$ become apparent if the metallicity is solar and the duration of shattering is longer than ~ 5 Myr. Therefore, when we treat a system in which the metallicity is solar and the star formation age is $\gtrsim 5$ Myr, we should take into account the effect of shattering in interstellar turbulence. In particular, the extinction curves of high- z quasars, whose metallicity is typically (above) solar, may be affected by shattering, and the UV rise of the extinction curve as well as the bump feature at $1/\lambda \sim 3.5\text{--}4 \mu\text{m}^{-1}$ can be attributed to the small grains produced by shattering. If the metallicity is $\lesssim 1/10$ solar, the extinction curve does not vary significantly on a time-scale of $\lesssim 10$ Myr because the frequency of grain–grain collisions is reduced in proportion to the grain abundance. Thus, the steepening mechanism of the extinction curve discussed in this paper is valid for systems whose metallicities are significantly greater than $1/10$ solar. We conclude that shattering in the WIM is generally of potential importance in starburst galaxies as a production mechanism of small grains.

ACKNOWLEDGMENTS

We thank the referee, A. P. Jones, for useful comments that improved this paper considerably. We thank T. T. Takeuchi and T. T. Ishii for helpful discussions. HY is supported by a TAP fellowship in Arizona. TN has been supported by the World Premier International Research Center Initiative (WPI Initiative), MEXT, Japan, and by a Grant-in-Aid for Scientific Research of the Japan Society for the Promotion of Science (19740094, 20340038).

REFERENCES

- Aannestad P. A., Kenyon S. J., 1979, *Ap&SS*, 65, 155
 Anders E., Grevesse N., 1989, *Geochim. Cosmochim. Acta*, 53, 197
 Bernard J.-P. et al., 2008, *ApJ*, 136, 919
 Bianchi S., Schneider R., 2007, *MNRAS*, 378, 973
 Bohren C. F., Huffman D. R., 1983, *Absorption and Scattering of Light by Small Particles*. Wiley, New York
 Borkowski K. J., Dwek E., 1995, *ApJ*, 454, 254
 Bot C. et al., 2004, *A&A*, 423, 567
 Bressan A., Fagotto F., Bertelli G., Chiosi C., 1993, *A&AS*, 100, 647
 Calzetti D., 2001, *PASP*, 113, 1449
 Dopita M. A. et al., 2005, *ApJ*, 619, 755
 Draine B. T., Anderson N., 1985, *ApJ*, 292, 494
 Dwek E., Galliano F., Jones A. P., 2007, *ApJ*, 662, 927
 Elmegreen B. G., Scalo J., 2004, *ARA&A*, 42, 211
 Galliano F., Madden S. C., Jones A. P., Wilson C. D., Bernard J.-P., 2005, *A&A*, 434, 867
 Gauger A., Balega Y. Y., Irrgang P., Osterbart R., Weigelt G., 1999, *A&A*, 346, 505
 Groenewegen M. A. T., 1997, *A&A*, 317, 503
 Guillet V., Pineau des Forêts G., Jones A. P., 2007, *A&A*, 476, 263
 Guillet V., Jones A. P., Pineau des Forêts G., 2009, *A&A*, 497, 145
 Hirashita H., Hunt L. K., 2004, *A&A*, 421, 555
 Hirashita H., Yan H., 2009, *MNRAS*, 394, 1061 (HY09)
 Hirashita H., Nozawa T., Kozasa T., Ishii T. T., Takeuchi T. T., 2005, *MNRAS*, 357, 1077
 Hirashita H., Nozawa T., Takeuchi T. T., Kozasa T., 2008, *MNRAS*, 384, 1725
 Hunt L. K., Hirashita H., 2009, *A&A*, 507, 1327
 Hunt L. K., Vanzil L., Thuan T. X., 2001, *A&A*, 377, 66
 Inoue A. K., 2005, *MNRAS*, 359, 171
 Inoue A. K., Hirashita H., Kamaya H., 2000, *PASJ*, 52, 539
 Jones A. P., Tielens A. G. G. M., Hollenbach D. J., McKee C. F., 1994, *ApJ*, 433, 797
 Jones A. P., Tielens A. G. G. M., Hollenbach D. J., 1996, *ApJ*, 469, 740
 Juarez Y., Maiolino R., Mujica R., Pedani M., Marinoni S., Nagao T., Marconi A., Oliva E., 2009, *A&A*, 494, L25
 Kawara K., Hirashita H., Nozawa T., Kozasa T., Oyabu S., Matsuoka Y., Shimizu T., 2010, *MNRAS*, submitted
 Kennicutt R. C., Jr, 1984, *ApJ*, 287, 116
 Kozasa T., Hasegawa H., Nomoto K., 1989, *ApJ*, 344, 325
 McKee C. F., 1989, in Allamandola L. J., Tielens A. G. G. M., eds, *IAU Symp. 135, Interstellar Dust*. Kluwer, Dordrecht, p. 431
 McKee C. F., Ostriker J. P., 1977, *ApJ*, 218, 148
 McKee C. F., Hollenbach D. J., Seab C. G., Tielens A. G. G. M., 1987, *ApJ*, 318, 674
 Maiolino R., Oliva E., Ghinassi F., Pedani M., Mannucci F., Mujica R., Juarez Y., 2004a, *A&A*, 420, 889
 Maiolino R., Schneider R., Oliva E., Bianchi S., Ferrara A., Mannucci F., Pedani M., Roca Sogorb M., 2004b, *Nat*, 431, 533
 Mathis J. S., 1990, *ARA&A*, 28, 37
 Mathis J. S., Ruml W., Nordsieck K. H., 1977, *ApJ*, 217, 425 (MRN)
 Nozawa T., Kozasa T., Umeda H., Maeda K., Nomoto K., 2003, *ApJ*, 598, 785
 Nozawa T., Kozasa T., Habe A., 2006, *ApJ*, 648, 435

Nozawa T., Kozasa T., Habe A., Dwek E., Umeda H., Tominaga N., Maeda K., Nomoto K., 2007, *ApJ*, 666, 955 (N07)
 O'Donnell J. E., Mathis J. S., 1997, *ApJ*, 479, 806
 Paradis D. et al., 2009, *AJ*, 138, 196
 Pei Y. C., 1992, *ApJ*, 395, 130
 Salpeter E. E., 1955, *ApJ*.
 Sellgren K., 1984, *ApJ*, 277, 623
 Serra Díaz-Cano L., Jones A. P., 2008, *A&A*, 492, 127
 Shull J. M., 1977, *ApJ*, 215, 805
 Slavin J. D., Jones A. P., Tielens A. G. G. M., 2004, *ApJ*, 614, 796
 Takeuchi T. T., Ishii T. T., Nozawa T., Kozasa T., Hirashita H., 2005, *MNRAS*, 362, 592
 Todini P., Ferrara A., 2001, *MNRAS*, 325, 726
 Umeda H., Nomoto K., 2002, *ApJ*, 565, 385
 Valiante R., Schneider R., Bianchi S., Andersen A. C., 2009, *MNRAS*, 397, 1661
 Yan H., Lazarian A., 2003, *ApJ*, 592, L33
 Yan H., Lazarian A., Draine B. T., 2004, *ApJ*, 616, 895
 Young J. S., Schloerb F. P., Kenney J. D., Lord S. D., 1986, *ApJ*, 304, 443

APPENDIX A: TEST FOR THE ‘ONE-SPECIES’ METHOD

As stated in Section 2.3, all grain species other than carbonaceous grains are treated as a single species, formally termed ‘silicate’ in calculating the grain-size distribution. This approximation is called the ‘one-species’ method, and it is exact if all the grain species have the same shape of grain-size distribution. We expect that the one-species method will give a reasonable answer, as Si is dominant among the ‘silicate’ category. Although the ‘silicate’ species other than Si (we term these species non-Si grains) have minor contributions in grain mass, some of them have a significant contribution to the number of small-sized grains, which affect the UV slope of the extinction curve. Here we test the validity of the one-species method in comparison with the ‘individual-species method’ as explained below.

The ‘individual-species’ method adopts the grain-size distribution of individual species, and the evolution of the grain-size distribution is calculated separately for individual species (note that the

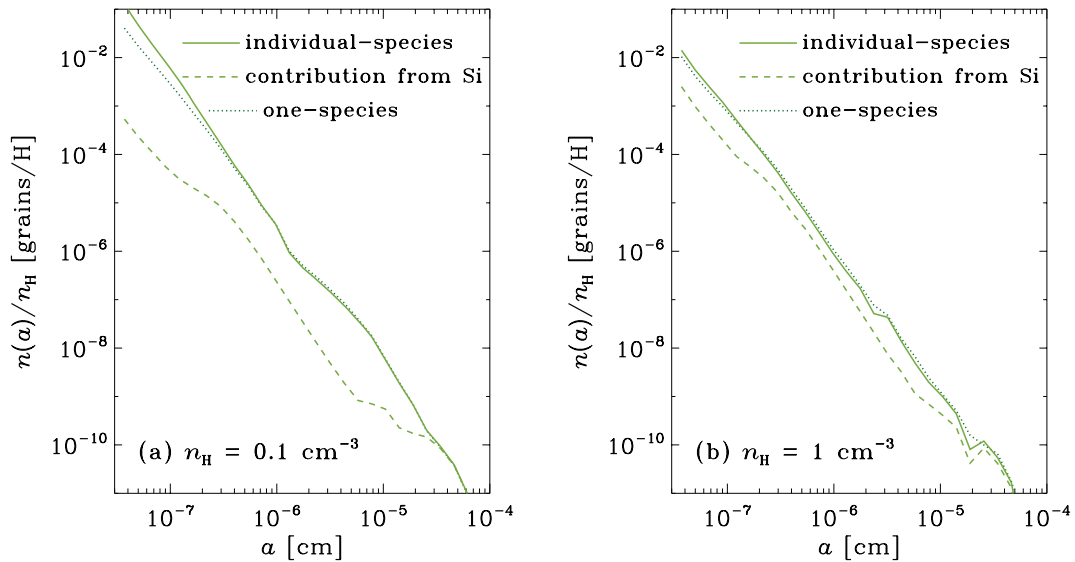


Figure A1. Size distributions for (a) $n_{\text{H}} = 0.1 \text{ cm}^{-3}$ and (b) $n_{\text{H}} = 1 \text{ cm}^{-3}$ for the grains other than carbon (i.e. ‘silicate’). The solid and dotted lines show the results with the individual-species method and with the one-species method, respectively. The dashed line represents the contribution from Si to the solid line. The metallicity and the age are assumed to be $1Z_{\odot}$ and 5 Myr, respectively.

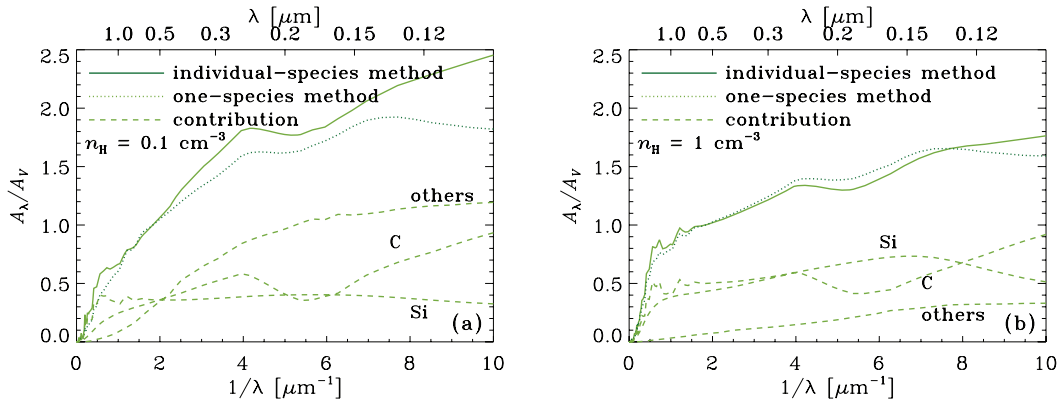


Figure A2. Extinction curves normalized to the V -band extinction for the grain-size distributions presented in Fig. A1 (the grain-size distributions of carbonaceous grains are the same as those in Figs 2 and 3). Panels (a) and (b) present the cases for $n_{\text{H}} = 0.1$ and 1 cm^{-3} , respectively. The solid and dotted lines show the results of the individual-species and one-species methods, respectively. The dashed lines represent the contributions from various species (C, Si and others, as labelled) for the individual-species method.

grain-size distribution summed over all species other than carbonaceous grains is adopted for ‘silicate’ in the one-species method). In calculating the evolution of the grain-size distribution of a certain species, the total mass density of the species relative to the gas density is assumed to be the total dust-to-gas ratio (but the grain-size distribution after shattering is normalized again to recover the correct mass ratio of each species). This treatment maximizes the production of small grains for non-Si species, which have smaller sizes than Si, but minimizes the production of small Si grains. Thus, this method is suitable for examining the maximum possible contribution from non-Si small grains to the UV extinction curve.

In Fig. A1, we compare the grain-size distributions predicted by the one-species and individual-species methods for $n_{\text{H}} = 0.1$ and 1 cm^{-3} at 5 Myr. For $n_{\text{H}} = 10 \text{ cm}^{-3}$, the difference between the two methods is negligible because non-Si grains contribute little to the total grain abundance. From the figure, we observe that the difference is relatively large in the case of $n_{\text{H}} = 0.1 \text{ cm}^{-3}$. This is because the fraction of non-Si grains is larger for $n_{\text{H}} = 0.1 \text{ cm}^{-3}$ than for $n_{\text{H}} = 1 \text{ cm}^{-3}$.

In Fig. A2, we show the extinction curves calculated by the two methods. We observe that the extinction curves of the individual-species method tend to be steeper than those of the one-species method. As can be seen in the figure, the steeper slope comes from the contribution from the non-Si grains, indicated by ‘others’. In the individual-species method, the size distribution of each non-Si species, which has a larger fraction of small grains than that of Si, is calculated separately, so that the production of small non-Si grains is enhanced. We note that the ‘real’ grain-size distribution would lie between the results of the two methods. This means that the approximate treatment adopted in the text (i.e. one-species method) is justified for $n_{\text{H}} \gtrsim 1 \text{ cm}^{-3}$. For $n_{\text{H}} \lesssim 0.1 \text{ cm}^{-3}$, because the contribution from non-Si species is significant, the error of the one-species method is at most ~ 10 per cent at $\lambda \sim 0.2 \mu\text{m}$, and ~ 40 per cent at $\lambda \sim 0.1 \mu\text{m}$. In order to overcome this uncertainty, we should develop a different scheme that could treat the collisions between multiple species (in our case, nine species), which cannot be treated in the current scheme in a reasonable computational time.

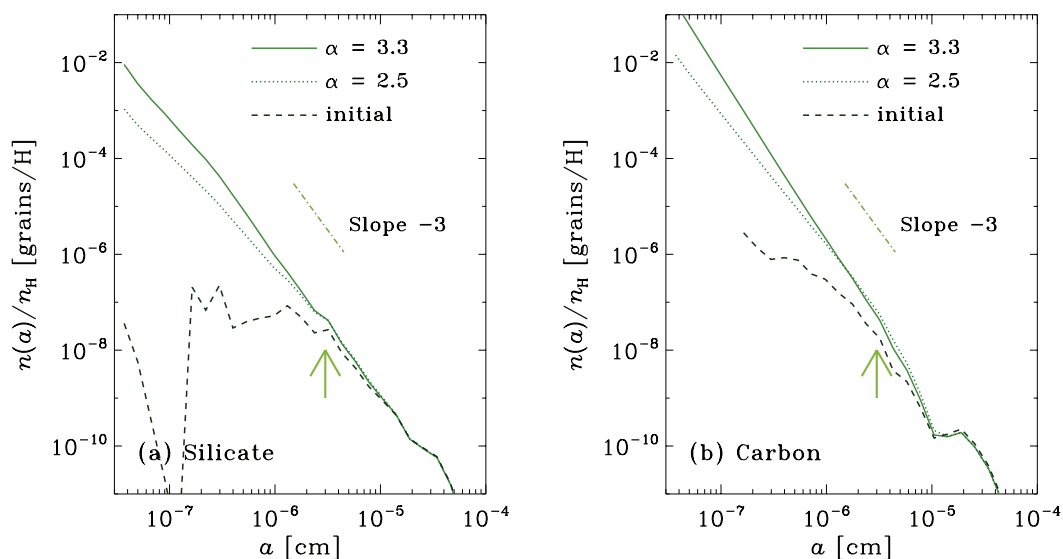


Figure B1. Grain-size distributions for $n_{\text{H}} = 1 \text{ cm}^{-3}$ with a metallicity of $1Z_{\odot}$. The solid and dotted lines show the results at $t = 5 \text{ Myr}$ for $\alpha_f = 3.3$ and 2.5 , respectively. The dashed line represents the initial grain-size distribution before shattering. Two grain species, (a) silicate and (b) carbonaceous dust, are shown. The arrow at $a = 0.03 \mu\text{m}$ indicates a rough representative size of the grains contributing to the steepening of the UV extinction curve.

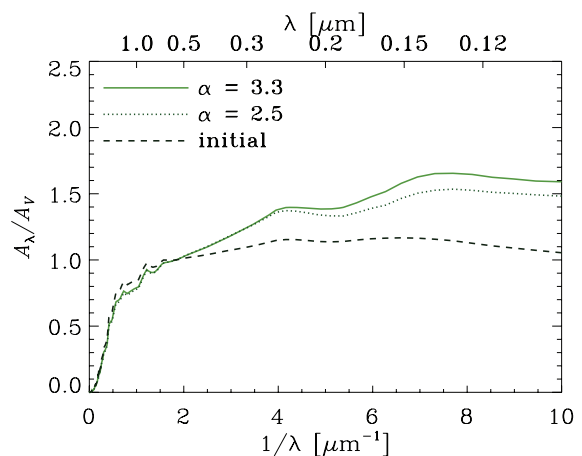


Figure B2. Extinction curves normalized to the V-band extinction for the grain-size distributions presented in Fig. B1. The solid and dotted lines show the results for $\alpha_f = 3.3$ and 2.5 , respectively. The dashed line represents the initial extinction curve before shattering.

APPENDIX B: FRAGMENT-SIZE DISTRIBUTION WITH A SHALLOWER SLOPE

The size distribution of shattered fragments is assumed to be a power law with an exponent of $-\alpha_f$. As discussed in the text, the steepening of the extinction curve becomes prominent if the power-law exponent (p) of the grain-size distribution around $a \sim 0.03 \mu\text{m}$ is steeper than ~ 3 (Section 4.1). Jones et al. (1996) have shown that the size distribution after shattering is not sensitive to α_f . They also argue that α_f slightly larger than 3 is robust against the change of the cratering flow parameters in shattering ($\alpha_f = 3.3$ is adopted in the text). Nevertheless, it would be interesting to examine whether $p > 3$ is realized even if we assume $\alpha_f < 3$.

Here we examine the smallest exponent adopted in Jones et al. (1996), $\alpha_f = 2.5$, as an extreme case. The ambient hydrogen number density is fixed at $n_{\text{H}} = 1 \text{ cm}^{-3}$. In Fig. B1, we show the result at $t = 5 \text{ Myr}$. As expected, the effect of α_f is more prominent for

smaller grains, as shattering with large α_f can supply small grains more efficiently. However, we observe that the difference between $\alpha_f = 2.5$ and 3.3 is small around $a \sim 0.03 \mu\text{m}$, confirming the result of Jones et al. (1996). The small difference comes from the fixed shattered mass in a collision; that is, the distribution of grain fragments as a function of size has a minor effect compared with the total mass of shattered fragments (shattering efficiency).

The extinction curves are shown in Fig. B2. We observe that the difference between the two curves with $\alpha = 2.5$ and 3.3 is negligibly small at $\lambda \sim 0.3 \mu\text{m}$ and is less than 10 per cent even at $\lambda \sim 0.1 \mu\text{m}$. The small difference is the natural consequence of the small variation of the grain-size distribution at $a \gtrsim 0.03 \mu\text{m}$.

This paper has been typeset from a $\text{\TeX}/\text{\LaTeX}$ file prepared by the author.